Adaptive Compensation of Dominant Frequency Components of Non-Repeatable Runout in Hard Disk Drives

Qixing Zheng and Masayoshi Tomizuka

Department of Mechanical Engineering

University of California at Berkeley, Berkeley, California 94720, U.S.A.

qiz@me.berkeley.edu, tomizuka@me.berkeley.edu

Abstract

This report is concerned with the non-repeatable runout (NRRO) compensation problem for hard disk drives. After standard servo control, several visible frequency components remain in the spectrum of non-repeatable PES. We call the frequency component with the largest magnitude as the dominant frequency component of NRRO. The spectral analysis of the dominant component reveals that its frequency varies at different location and its magnitude and phase are time-varying. The existing loop shaping compensation scheme for this disturbance introduces a notch at the center frequency of the dominant component to the sensitivity function to achieve certain attenuation at this frequency. With this conventional compensation scheme, the dominant component can only be reduced by 50%. In this report, we propose a new compensation scheme to completely reject the dominant

component. Its frequency is estimated on-line by the least mean squares (LMS) algorithm within a short time window. Based on the frequency estimate, the basis function algorithm is applied to adaptively identify the time-varying magnitude and phase of the dominant component. With the identified frequency, magnitude and phase, an estimate of the dominant component is constructed and then canceled by the control signal. This scheme is further extended to compensating for multiple frequency components. The performance of this compensation scheme is demonstrated by simulation on a realistic hard disk drive model.

Keywords: Basis function algorithm, frequency identification, hard disk drives, non-repeatable runout, time-varying sinusoidal signal.

1. Introduction

The constantly growing track density of hard disk drives (HDD's) requires more and more accurate positioning of the read/write head, i.e., more and more stringent track mis-registration (TMR) budget. The source of TMR is the disturbance in HDD, including repeatable runout (RRO) and non-repeatable runout (NRRO). Then the increase in the track density involves reducing these two TMR sources.

RRO and NRRO are totally different in nature. RRO is locked to the spindle rotation in both frequency and phase. RRO can be rejected either by improving the precision of the servo-writer during the manufacturing processes or by servo control algorithms, like repetitive

control [1] and adaptive feedforward control [2]. Unlike RRO, NRRO contains frequency components with time-varying phases and magnitudes at unknown frequencies. We call the frequency component with the largest magnitude in the power spectrum of the non-repeatable PES (the PES caused by NRRO) as the dominant frequency component of NRRO as shown in Fig. 1. NRRO can be rejected by improving the mechanical design, like an improved spindle motor using damping material [3]. This time-consuming re-design of mechanical component, however, will significantly increase the cost of disk drives. The other way to handle NRRO is via the servo system. Kim et al. proposed a control strategy to deal with the NRRO caused by the mechanical vibration of the disk [4]. They added a 2nd order peak filter to the servo loop in parallel with the existing controller to achieve certain attenuation at the center frequency of the filter. With this compensation scheme, the dominant component was reduced by 50% and the TMR improvement was limited.

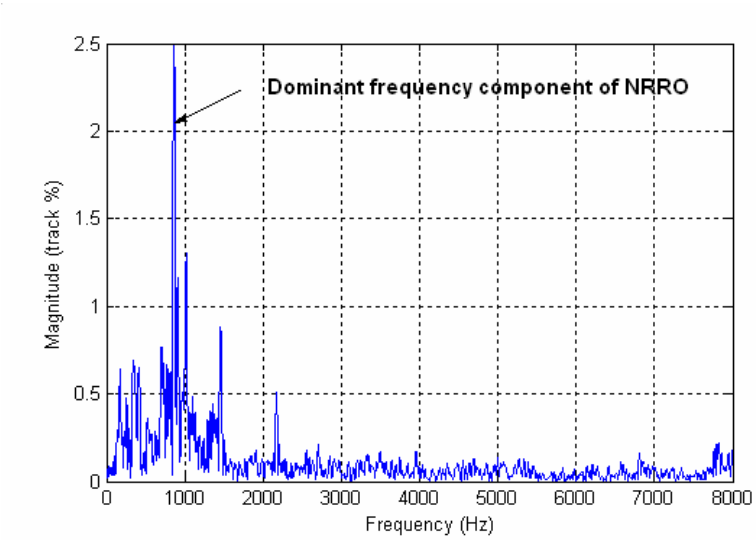

Fig. 1 An example of non-repeatable PES spectrum after standard servo control.

In this report, we propose a new compensation scheme for NRRO. The structure of this scheme is shown in Fig. 2. *P* represents the hard disk drive, including power amplifier, voice

coil motor (VCM), and head stack assembly (HSA). The standard servo controller *C* is a PID controller cascaded with a notch filter tuned not to excite the dominant resonant mode. With this controller alone, we have some visible frequency components with large magnitude in the spectrum of the non-repeatable PES as shown in Fig. 1. To reject the dominant frequency component, a compensator (depicted in dashed box in Fig. 2) is added on top of the original controller. This compensator first involves estimation of the frequency of the dominant component within a short time window from the PES. Based on the frequency estimate, the time-varying magnitude and the time-varying phase of the dominant component are adaptively estimated by the basis function algorithm [1]. Then the estimated dominant component (v(k) in Fig. 2) is removed from the control signal.

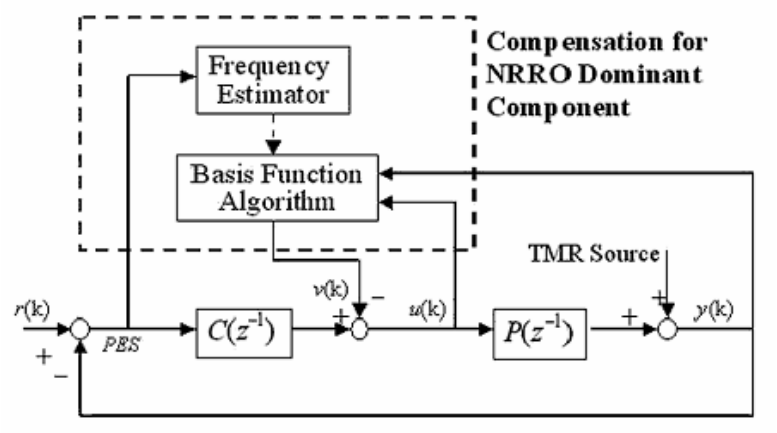

Fig. 2. Structure of adaptively rejecting NRRO dominant component.

The remainder of this report is organized as follows. In Section 2, more details of the dominant frequency component of NRRO are revealed. A simple method of frequency estimation of the dominant component is introduced in Section 3. The basis function algorithm for identifying the magnitude and the phase of the dominant component is presented in Section 4. Section 5 shows the performance of this compensation scheme by

simulation on a realistic HDD model with the TMR source collected from a commercial disk drive. In Section 6 we extend this compensation scheme to compensate for multiple frequency components and demonstrate its performance by simulation. The conclusion is drawn in Section 7.

2. Dominant Frequency Component

The dominant frequency component is the largest one in the non-repeatable PES spectrum among many disk modes caused by disk flutter [5]. Disk flutter is the vibration in the axial direction of the disk due to internal windage excitation during the disk operation. This axial vibration can be translated to the head off-track in the radial direction and shows up as narrow band peaks in the non-repeatable PES spectrum. To make it worse, the head off-track concentrated in [350 Hz, 2000 Hz] is amplified by the error rejection function (the transfer function from the TMR source to the plant output $y(k)$) [5]. This amplification along with the rapid growth in track density and spindle motor speed makes disk flutter a major contribution to NRRO.

There exist many mechanical approaches to suppressing disk flutter. Examples of such mechanical re-design include novel aerodynamic designs of the shroud (like decreasing disk-to-shroud spacing [6], smoothening the shroud contour and reducing the shroud opening [7]), squeeze air bearing damping [8], feedback [9] and feedforward [10] control using additional sensors, feedback control with piezoelectric actuator patches [11], and

optimal HSA design [12]. Most of these approaches yield significant TMR reduction. However, these modified mechanical structures of HDD will greatly increase the cost of disk drives. Instead, we propose an adaptive scheme to reject the dominant frequency component due to disk flutter involving only servo re-design.

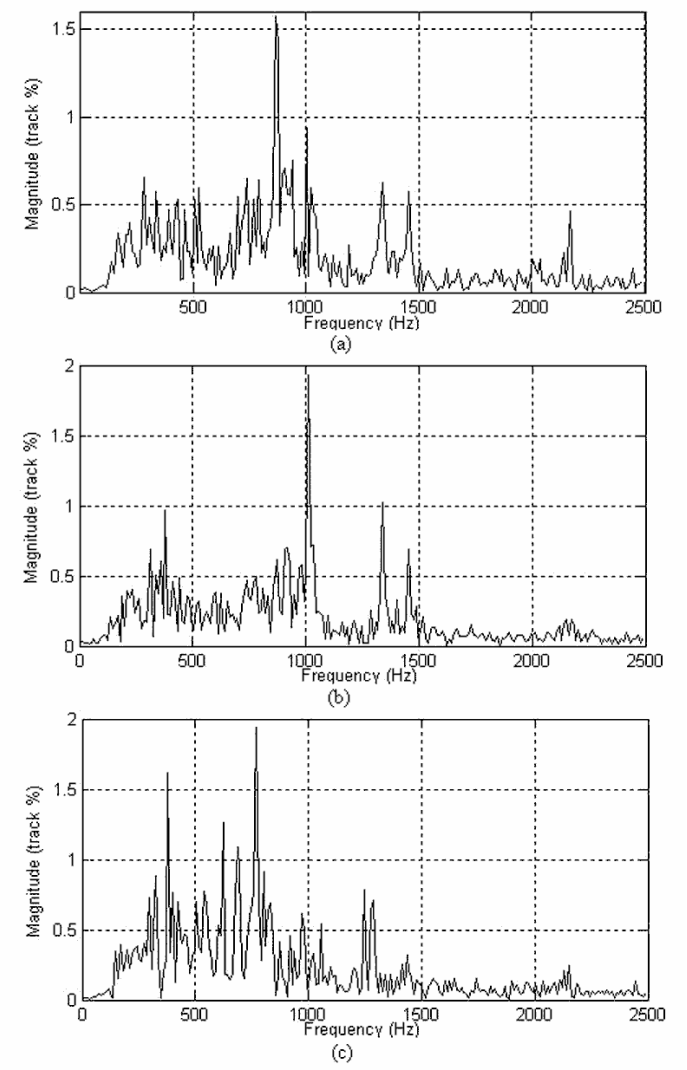

Fig. 3. The power spectrum of non-repeatable PES in three different zones: (a) In zone No.1 (dominant component exists at 870Hz);(b) In zone No.2 (at 1000Hz); (c) In zone No.3 (at 750Hz).

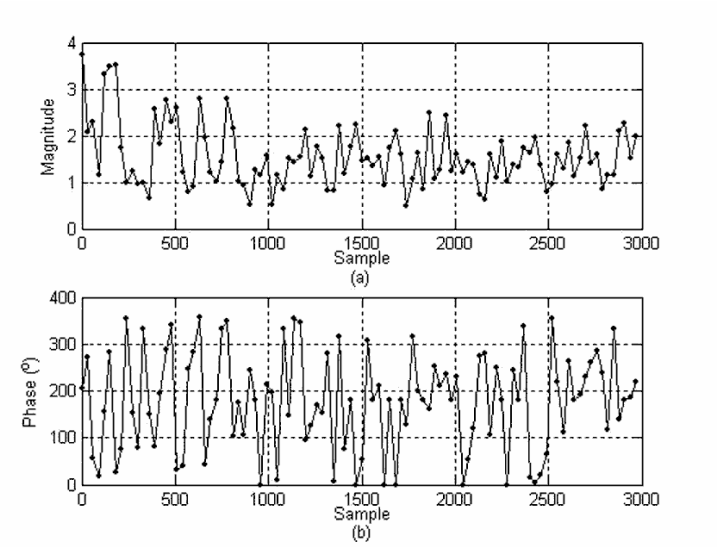

Fig. 4. Spectral analysis (discrete Fourier transform) of the dominant component in every 30 sample non-repeatable PES: (a) Time trace of magnitude; (b) Time trace of phase.

To reject the dominant component of NRRO, it is required to know its nature in frequency-domain. Figure 3 shows that the frequency of the dominant component varies from one zone to another (different head or different track). The magnitude and the phase are both time-varying for the dominant component in a fixed zone as depicted in Fig. 4. Therefore, the dominant frequency component of NRRO can be modeled as a sinusoidal signal with time-varying magnitude and phase at varying frequency for different zones in a HDD.

3. Frequency Identification

The frequency of the dominant component needs be identified on-line, because it varies

from track to track. Furthermore, since the read-write head does not stay on one track for many revolutions during operation, the frequency identification should be completed within a short time window.

For fast on-line frequency identification, the PES is filtered by a band pass filter shown in Fig. 5 to isolate the frequency band of the dominant component from other components as well as to enhance the signal-to-noise ratio (SNR) for identification. The dominant component is assumed to reside in certain frequency band: [700Hz, 1100Hz] in our case. The filtered PES is then used for the frequency identification.

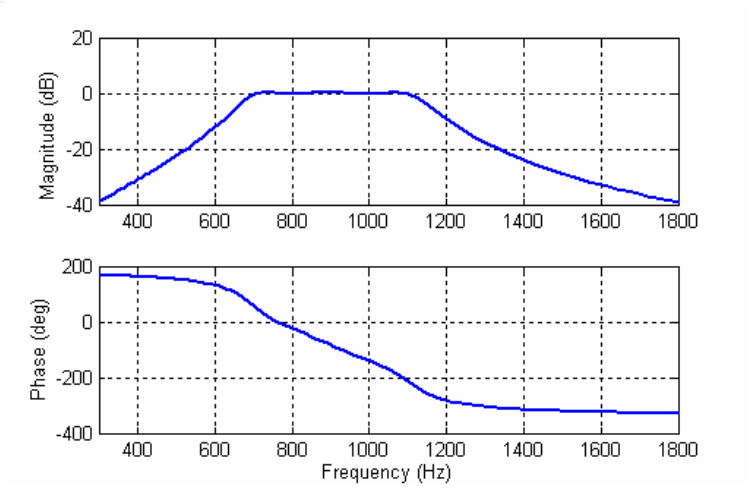

Fig. 5. Frequency response of the band pass filter for the frequency identification. The frequency range [700 Hz, 1100 Hz] is contained in the pass band.

The most accurate and straightforward method for the frequency identification is spectral analysis, which requires discrete Fourier transform of the filtered PES. The dominant component is at the frequency where the largest peak resides in the spectrum. Spectral analysis, however, is not suited for on-line identification due to its impractically large

amount of computation for doing discrete Fourier transform. In this report, the on-line frequency identification is achieved by the computationally simple LMS algorithm.

Let $z(k)$ and $x(k)$ represent the filtered PES and the dominant frequency component, respectively. All other frequency components contained in $z(k)$ are treated as noise $n(k)$, i.e., $z(k) = x(k) + n(k)$. Noticing that the dominant frequency component $x(k)$ is actually a sinusoidal signal, which satisfies

$$x(k) = 2\cos(\omega)x(k-1) - x(k-2), \tag{1}$$

where ω is the frequency (in rad/sec) of the dominant component, we can define the estimation error as

$$e(k) = z(k) + z(k-2) - \hat{\lambda}(k)z(k-1), \tag{2}$$

where $\hat{\lambda}(k)$ is defined as

$$\hat{\lambda}(k) = 2\cos\left[\hat{\omega}(k)\right]. \tag{3}$$

Then the estimate of this frequency coefficient can be obtained by the LMS algorithm [13]:

$$\hat{\lambda}(k+1) = \hat{\lambda}(k) - \mu \frac{\partial e(k)}{\partial \hat{\lambda}(k)} e(k), \tag{4}$$

where μ is the step size and $e(k)$ is the estimation error defined in (2). Noticing that

$$\frac{\partial e(k)}{\partial \hat{\lambda}(k)} = -z(k-1), \tag{5}$$

$\hat{\lambda}(k)$ is finally updated according to

$$\hat{\lambda}(k+1) = \hat{\lambda}(k) + \mu\, z(k-1)e(k). \tag{6}$$

Then the frequency estimate at the (k+1)-th sample is given by

$$\hat{\omega}(k+1) = \cos^{-1}[\hat{\lambda}(k+1)/2]. \tag{7}$$

A non-rigorous proof of the stability and convergence of this algorithm of frequency identification is provided as follows.

Let λ denote the true value of the frequency coefficient, i.e., $\lambda = 2\cos(\omega)$. Suppose that $z(k)$ can be expressed as

$$\begin{aligned} z(k) &= 2\cos(\omega)z(k-1) - z(k-2) + \xi(k) \\ &= \lambda z(k-1) - z(k-2) + \xi(k) \end{aligned}, \tag{8}$$

where $\xi(k)$ is considered as the modeling error of $z(k)$. After subtracting λ from the both sides of (6), substituting $e(k)$ by (2) and substituting $z(k)$ by (9), we can get the dynamic model of the frequency coefficient error $\bar{\lambda}(k) = \hat{\lambda}(k) - \lambda$ as

$$\bar{\lambda}(k+1) = (1 - \mu[z(k-1)]^2)\bar{\lambda}(k) + \mu\, z(k-1)\xi(k). \tag{9}$$

The PES in HDD is bounded and so is the filtered PES $z(k)$. Since $\xi(k)$ depends only on $z(k)$, $z(k-1)$, $z(k-2)$, and λ, it must also be bounded. Therefore, there exists a positive constant *M* satisfying $|z(k-1)\xi(k)| \le M$ for all *k*.

Suppose that

$$\left|1 - \mu[z(k-1)]^2\right| \le \eta, \tag{10}$$

for all *k* and some positive constant η. Then we have

$$\left|\bar{\lambda}(k+1)\right| \le \eta\left|\bar{\lambda}(k)\right| + \mu M, \tag{11}$$

which yields an upper bound for $\left|\bar{\lambda}(k)\right|$:

$$\left|\bar{\lambda}(k)\right| \le C\eta^k + \frac{\mu M}{1-\eta}, \tag{12}$$

where constant C depends on the initial absolute error $\left|\bar{\lambda}(0)\right|$. Thus, if the step size μ satisfies

$$0 < \mu < \frac{2}{\max_k [z(k)]^2}, \tag{13}$$

then $\eta < 1$ and

$$\lim_{k\to\infty} \left|\bar{\lambda}(k)\right| \le \frac{\mu M}{1-\eta}. \tag{14}$$

The bound in (14) can be made small by choosing small μ, whereas large μ (but still less than $(\max_k [z(k)]^2)^{-1}$) is desired for fast convergence.

On the other hand, $z(k)$ can be considered as a random process with bounded value. Suppose that (10) still holds. Then from (9), we have

$$E(\left|\bar{\lambda}(k+1)\right|) \le \eta E(\left|\bar{\lambda}(k)\right|) + \mu\, E(\left|z(k-1)\xi(k)\right|). \tag{15}$$

If $\mu E(\left|z(k-1)\xi(k)\right|) = 0$, then $\hat{\lambda}(k)$ is an asymptotically unbiased estimate of λ. Since $\mu E(\left|z(k-1)\xi(k)\right|)$ is small in our case, the bias of $\hat{\lambda}(k)$ is also small.

The frequency estimation converges within one revolution by this LMS algorithm with small amount of computation and the converged frequency estimate is used for the magnitude and phase identification. The detail of simulation result is shown in Section 5.

4. Magnitude and Phase Identification

For magnitude and phase identification, it is convenient to let the disturbance (TMR source) enter at the input to the plant as shown in Fig. 6. Here we suppose that the transfer function of the plant is

$$P(z^{-1}) = \frac{z^{-d} B(z^{-1})}{A(z^{-1})}. \tag{16}$$

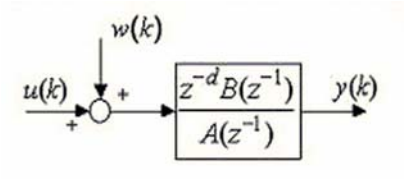

Fig. 6. Plant model with disturbance at input.

A delayed estimate of the disturbance can be generated by inverting the plant transfer function without the pure delay. When there are unstable zeros in the plant, the zero-phase error tracking algorithm [14] can be used to get approximate inversion. Suppose that the inverse of the plant is $P_{in}(z^{-1})$ ($P_{in}(z^{-1}) = A(z^{-1}) / B(z^{-1})$, if there are no unstable zeros). The disturbance estimate at $(k - d)$-th sample is then given by

$$w(k-d) = P_{in}(z^{-1}) y(k) - u(k-d). \tag{17}$$

With the identified frequency $\hat{\omega}$, we can employ a band pass filter given by

$$G_{bpf}(z) = (1-r)\frac{z^2 - r}{z^2 - 2r\cos(\hat{\omega}) z + r^2} \tag{18}$$

to get rid of the frequency components other than the dominant one contained in $w(k-d)$. Notice that at $\hat{\omega}$, $G_{bpf}(z)=1$, which guarantees that at the steady state the filtering does not change the magnitude and the phase of the dominant component and by making r close to and less than 1, we have a narrow pass band. Then the filtered $w(k-d)$ (denoted by $w'(k-d)$) is approximately equal to $x(k-d)$.

The time-varying phase and magnitude of $x(k-d)$ are identified using the basis function algorithm in [1], which is based on a Fourier expansion of the dominant component

$$\begin{aligned} x(k-d) &= \alpha\cos[(k-d)\hat{\omega}] + \beta\sin[(k-d)\hat{\omega}] \\ &= \Theta^T\Phi(k-d), \end{aligned} \tag{19}$$

where $\Phi^T(k)=[\cos(\hat{\omega}k)\ \sin(\hat{\omega}k)]$, $\Theta^T=[\alpha\ \beta]$, and α and β are unknown coefficients, which are related to the magnitude and the phase of the dominant component. The objective is to correctly identify these coefficients in Θ. Let an estimate of Θ be denoted by

$$\hat{\Theta}^T(k)=[\alpha(k)\ \ \beta(k)]. \tag{20}$$

The a priori estimation error is defined by

$$\begin{aligned} \varepsilon^0(k) &= w'(k-d) - \hat{x}^0(k-d) \\ &\approx \Theta^T\Phi(k-d) - \hat{\Theta}^T(k-1)\Phi(k-d). \end{aligned} \tag{21}$$

The parameter estimate vector, $\hat{\Theta}^T(k)$, is updated at every sample using the recursive least squares parameter adaptation algorithm [15] as

$$\hat{\Theta}^T(k) = \hat{\Theta}^T(k-1) + \frac{F(k)\Phi(k-d)\varepsilon^0(k)}{1+\Phi^T(k-d)F(k)\Phi(k-d)} \tag{22}$$

$$F(k+1)=\frac{1}{\lambda_1}\left[F(k)-\frac{F(k)\Phi(k-d)\Phi^T(k-d)F(k)}{\lambda_1+\Phi^T(k-d)F(k)\Phi(k-d)}\right], \tag{23}$$

where λ_1 is the forgetting factor.

The convergence of $\hat{\Theta}^T(k)$ yields an accurate representation of the dominant component and this estimate, $\hat{x}(k)=\hat{\Theta}(k)\Phi(k)$, is removed from the input to the plant to compensate for the dominant frequency component by letting

$$v(k)=-\hat{x}(k)\,. \tag{24}$$

5. Simulation Results

The plant model used in simulation is a 27th order LTI system, which includes all the resonant modes at high frequency and behaves almost identically to a real disk drive. As in [16], the disturbance (TMR source) is obtained by filtering the PES collected from a commercially available HDD through $-S^{-1}(z^{-1})$, where $S(z^{-1})$ is the sensitivity function ($S(z^{-1})=1/[1+P(z^{-1})C(z^{-1})]$ for the original HDD system, which is the remaining feedback control system in Fig. 2 after the compensation part is removed). With the realistic plant model and the practical disturbance, our simulation results should be close to what we will get when this compensation algorithm is implemented in a real disk drive.

As described in Section 3, the performance of the frequency identification is determined

by the step size in the LMS algorithm: a large step size results in fast convergence and large fluctuation after convergence and vice versa. The frequency estimates for $\mu = 0.01$ and $\mu = 0.001$ are compared in Fig. 7. In the simulation, we allow one revolution for the frequency estimate to converge and use the estimated frequency at the end of the first revolution to do the magnitude and phase identification.

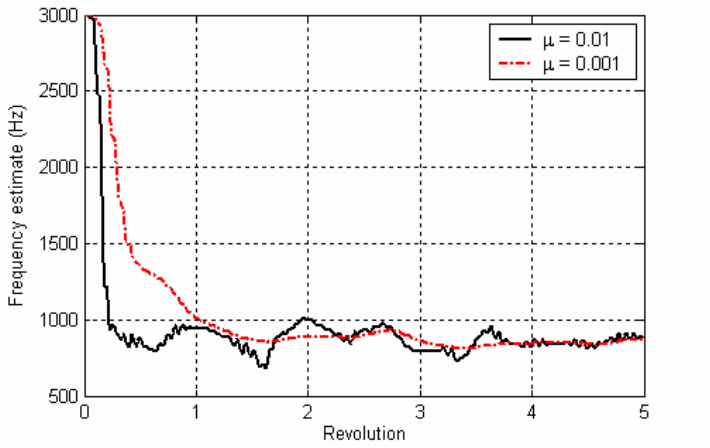

Fig. 7. Frequency identification by the LMS algorithm with different values of the step size.

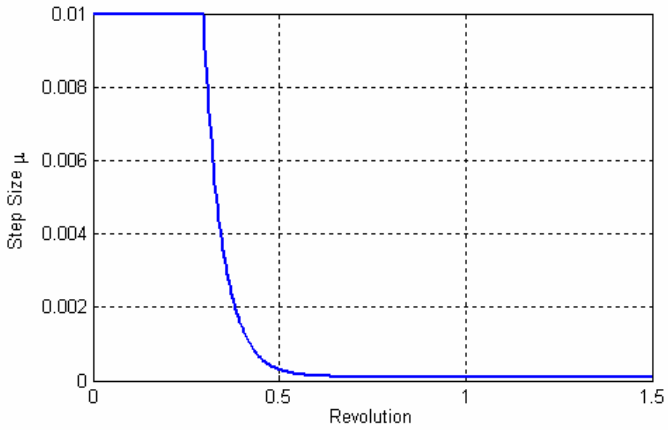

Fig. 8. Trajectory of the time-varying step size for frequency estimation.

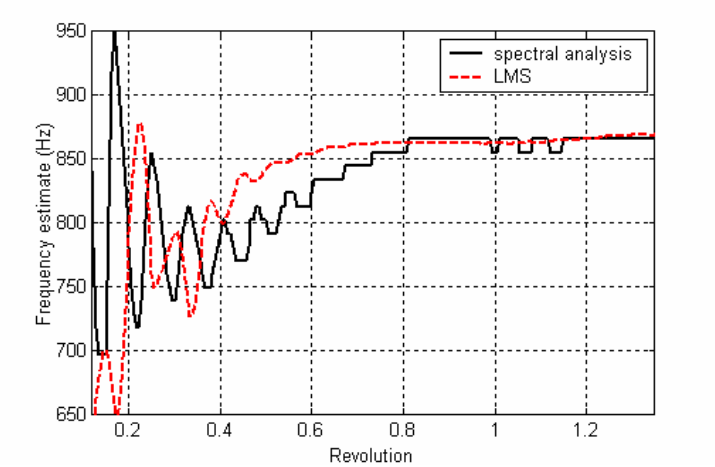

Fig. 9. Simulation result of the frequency identification by spectral analysis and by the LMS algorithm.

In order to achieve both fast convergence at the beginning and small fluctuation after convergence, we use a time-varying step size as depicted in Fig. 8. The step size μ remains 0.01 for the first 1/4 revolution, then it is ramped down, according to the equation

$$\mu(k+1) - 0.0001 = 0.9[\mu(k) - 0.0001]. \tag{21}$$

This makes μ exponentially converge to 0.0001. With this step size, the frequency estimate converges within one revolution and is similar to the result of spectral analysis (discrete Fourier transform) as shown in Fig. 9. The converged frequency estimate by the LMS algorithm after one revolution is 861 Hz, which is very close to 854 Hz, the frequency of the component with the largest magnitude in the spectrum of one revolution of the filtered PES. This identified frequency is then used to build the band pass filter in (18) and to run the basis function algorithm.

To see how the TMR is improved by the proposed compensation scheme, a simulation

was performed by running the basis function algorithm for five revolutions to reject the dominant frequency component. The first thing to do for the basis function algorithm is to compute the disturbance estimate using (17) by filtering the measurement or the output of the plant through the inverse of the plant. The inverse of the 27th order full plant model is not practical due to the large amount of computation. In the simulation, we use the inverse of a 4th order simplified plant model to get the disturbance estimate. The simplified plant model is a double-integrator with one major resonant mode at around 5,000 Hz. The magnitude and the phase of the simplified model differ from those of the full order model only at high frequencies. The inverse of the simplified plant works almost the same as the accurate inverse, since the difference at high frequencies is reduced by the band pass filter (18). The coefficient r in (18) is set to 0.98 in the simulation. The forgetting factor λ_1 of the recursive least squares parameter adaptation algorithm in (23) is chosen to be a small value 0.3 representing strong forgetting, since the magnitude and the phase of the dominant component vary fast.

Our compensation scheme is mainly for the track following performance, which means that the reference is zero ($r(k)=0$ in Fig. 2). In the spectrum of the PES shown in Fig. 10, we can see that the dominant component is almost completely removed by our compensation scheme with small amplification in [1300 Hz, 2300 Hz] and the TMR is reduced by 17% (the standard deviation of the PES before and after compensation are 3.36 and 2.78 in the unit of percent track, respectively).

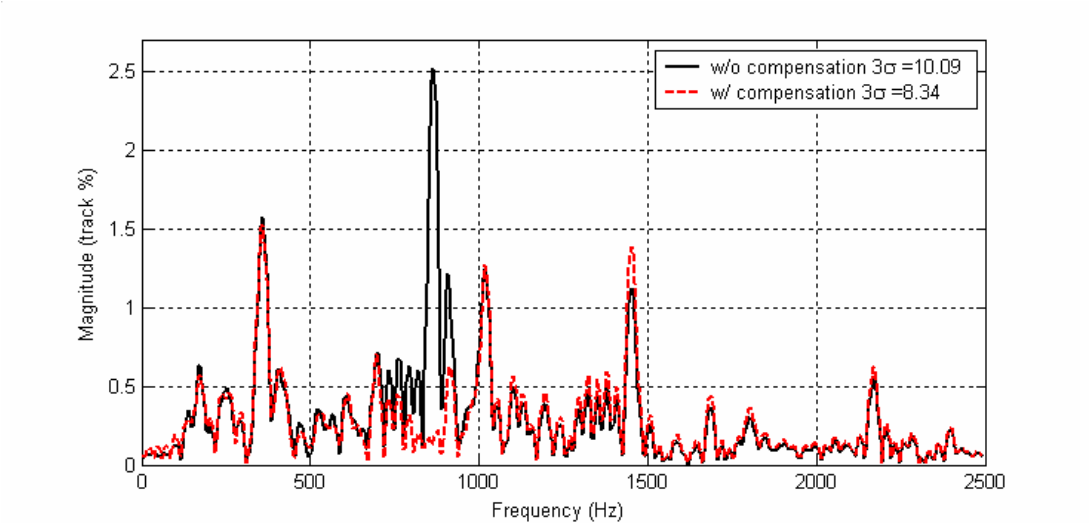

Fig. 10. PES spectrum before and after compensation.

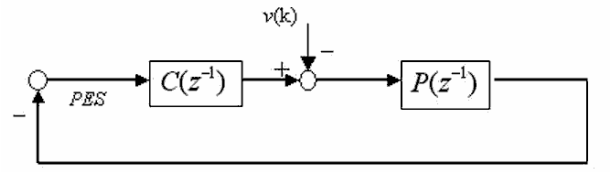

Fig. 11. Block diagram of the simulation system for checking the effect of the compensation.

It is important to confirm that the proposed scheme is capable to track the time-varying magnitude and phase of the dominant frequency component. This point was studied by simulation as follows. First, we obtain the time traces of magnitude and phase of the dominant component at 861 Hz in the original system (without compensation) as done in Fig. 4. Then run a simulation with compensation and store the compensation signal (v(k) in Fig. 2). To see the effect of the compensation signal, we simulate the system shown in Fig. 11 with the previously stored compensation signal as the only input, obtaining the time traces of magnitude and phase of the frequency component at 861 Hz in the negative PES. These time traces are then compared with the original time traces without compensation. As shown Fig. 12, the magnitude and the phase of the frequency component at 861 Hz in the negative PES

caused by the compensation signal alone are close to those of the dominant component of the uncompensated case. Because the system is linear, the dominant component is canceled by the compensation signal.

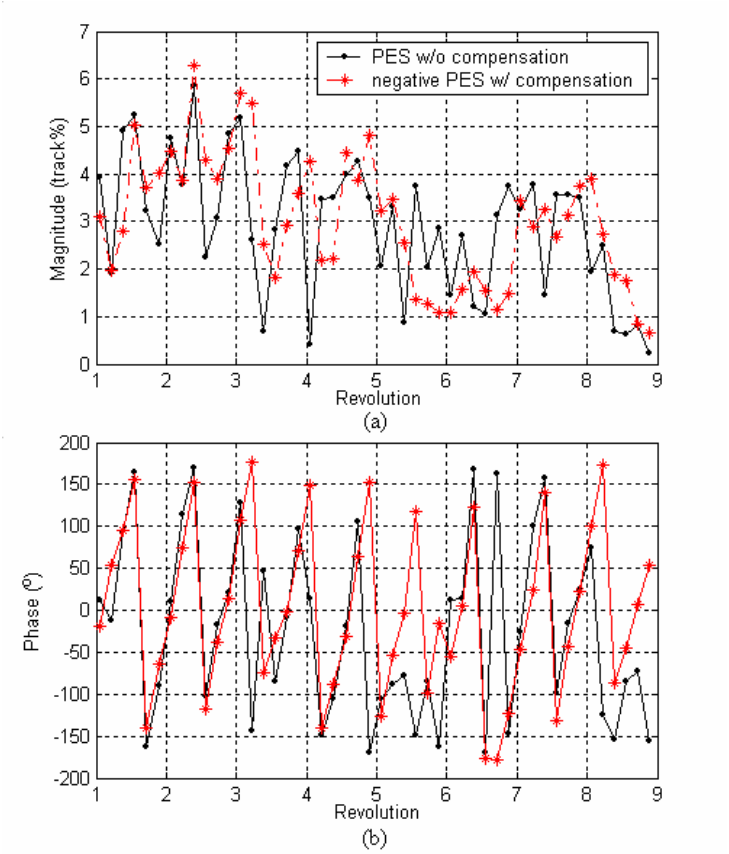

Fig. 12. Time traces of (a) magnitude and (b) phase of the frequency component at 861 Hz in the original PES spectrum and in the negative PES spectrum generated by the compensation signal.

6. Multiple Component Compensation

One advantage of the proposed compensation scheme is that it can be extended to deal with multiple frequency components. Figure 13 shows the structure of three component

compensation. We filter the PES by three band pass filters (one of which is actually a low pass filter) with disjoint pass bands as shown in Fig. 14 to select the frequency range of interest. Assume that in PES spectrum we have one dominant component in each pass band. Then each component can be removed by the single component compensation scheme introduced in the previous sections. The compensation blocks in Fig. 13 are identical to each other, involving frequency estimation by LMS and magnitude and phase identification using the basis function algorithm.

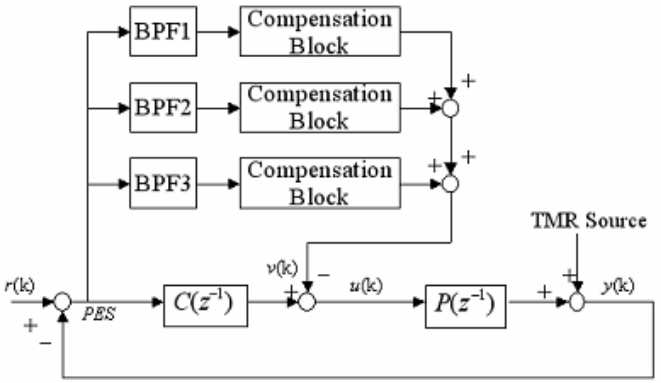

Fig. 13. Structure of multiple component compensation (BPF: band pass filter with different pass band).

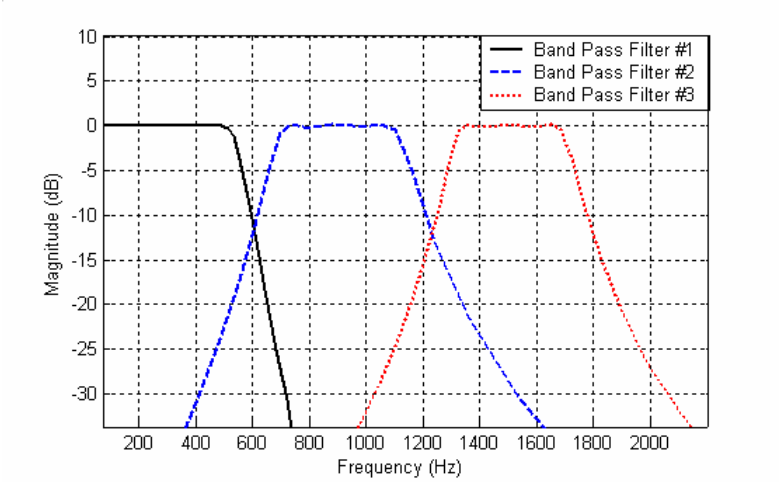

Fig. 14. Magnitude of the frequency responses of three band pass filters with disjoint pass bands [0 Hz, 500 Hz], [700 Hz, 1100 Hz], and [1300 Hz, 1700 Hz].

Suppose that we have a PES spectrum shown in Fig. 15(a). Component No.1 is the dominant one in frequency range [0 Hz, 500 Hz], No.2 in [700 Hz, 1100 Hz], and No.3 in [1300 Hz, 1700 Hz]. In Fig. 15(b) we can clearly see that the spectrum of the output of each band pass filter has only one dominant frequency component.

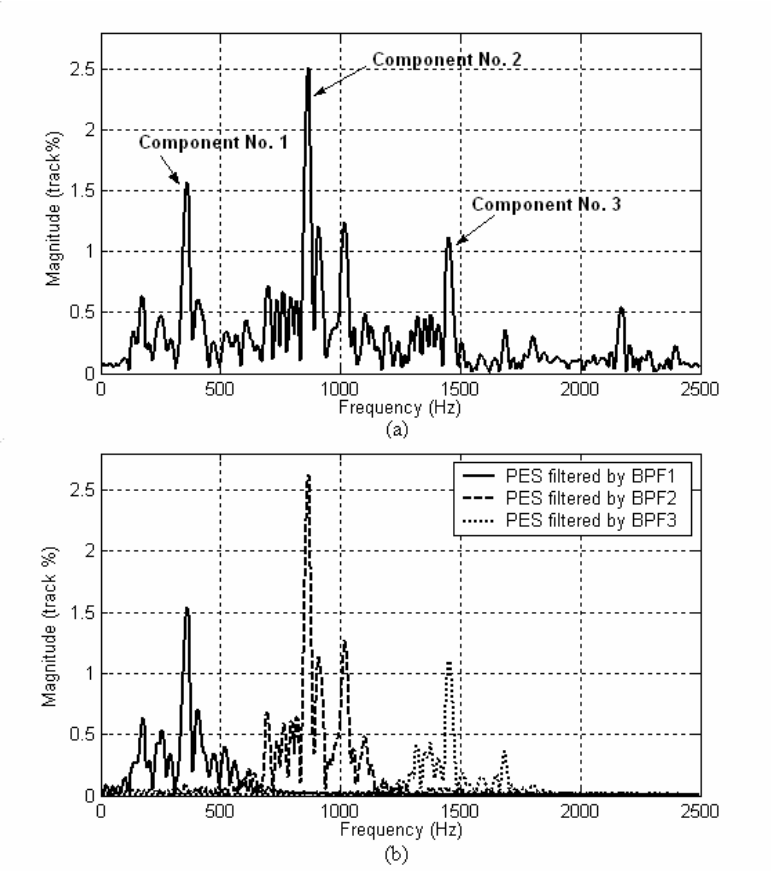

Fig. 15. PES spectra: (a) original; (b) filtered by different band pass filters.

Same as before, the first revolution of simulation is dedicated to the frequency identification by the LMS algorithm with time-varying step size. Figure 16 shows that the frequency estimate for every component converges within one revolution and is close to the result of spectral analysis. The converged frequency estimates for the three dominant components after one revolution are 377 Hz, 861 Hz, and 1468 Hz, respectively, which are all close to their true values 360 Hz, 854 Hz, and 1450 Hz. With these frequency estimates, the

magnitude and the phase of each dominant component are identified and then used to construct the compensation signal. We run the compensation for these three components for 5 revolutions and compare the PES spectrum with the original spectrum. As shown in Fig. 17, all three components have been greatly attenuated by the proposed compensation scheme and 25% TMR improvement is achieved in total (the standard deviation of the PES is reduced from 3.36 to 2.53 in the unit of percent track).

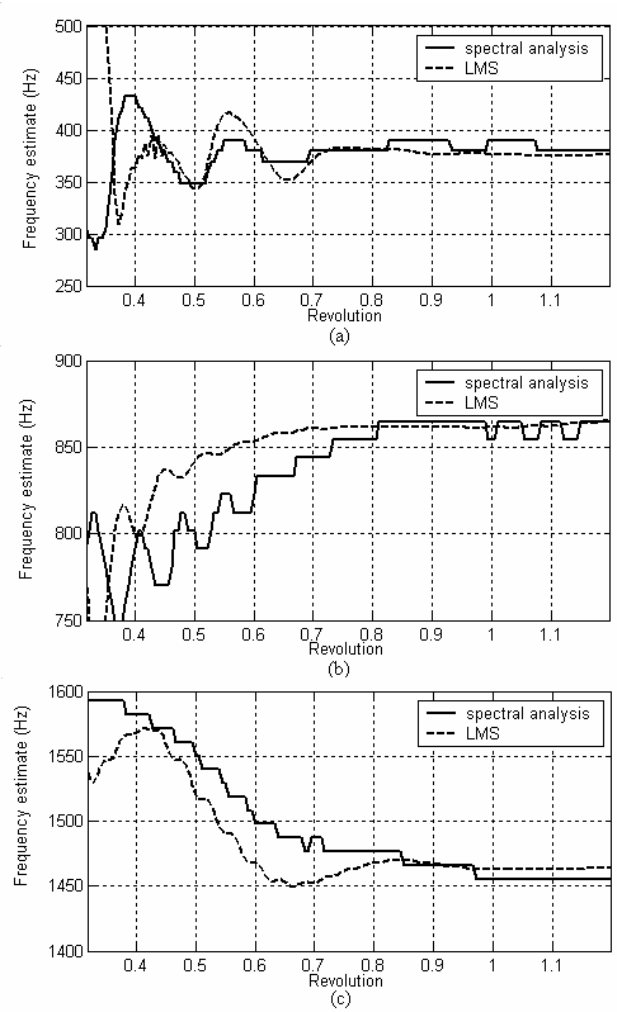

Fig. 16. Frequency identification for (a) Component No.1; (b) Component No.2; (c) Component No.3 by spectral analysis and by LMS.

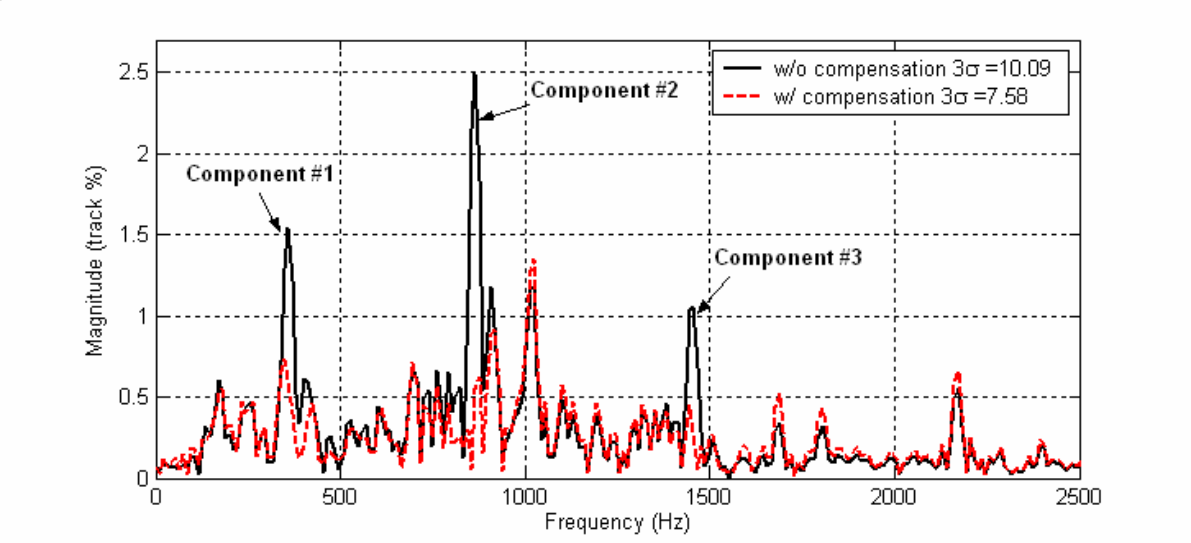

Fig. 17. PES spectrum with and without multiple component compensation

7. Conclusion

This report described a new compensation scheme for NRRO in HDD. This scheme involved two steps: identification of frequency and identification of magnitude and phase of the dominant frequency component. The frequency identification was done within one revolution by the LMS algorithm with time-varying step size and the basis function algorithm was used to adaptively identify the phase and the magnitude. Simulation result showed that the compensation tracked the time-varying magnitude and phase of the dominant component well and 17% TMR improvement could be achieved by single component compensation. This compensation method was then extended to handle three dominant components in three disjoint frequency ranges for larger TMR reduction (25%), which significantly enhanced the positioning accuracy of the read/write head and thus made higher TPI possible for the future HDD products.

Acknowledgement

This work was supported by the *Computer Mechanics Laboratory of the University of California, Berkeley*.

References

[1] C. Kempf, W. Messner, M. Tomizuka and R. Horowitz, "Comparison of four discrete-time repetitive control algorithms," *IEEE Control System Magazine*, vol. 13, no. 6, pp. 48-54, Dec. 1993.

[2] S. Wu and M. Tomizuka, "Repeatable runout compensation for hard disk drives using adaptive feedforward cancellation," in *2006 American Control Conference*, pp. 6, Piscataway, NJ, USA.

[3] G. Jang, S. Hong, D. Kim, and J. Han, "New design of a HDD spindle motor using damping material to reduce NRRO," *IEEE Transactions on Magnetics*, vol.36, no.5, pp. 2258-60, Sept. 2000.

[4] Y. Kim, C. Kang, and M. Tomizuka, "Adaptive and optimal rejection of non-repeatable disturbance in hard disk drives," in *2005 IEEE/ASME International Conference on Advanced Intelligent Mechatronics*, Monterey, vol. 1, pp. 1-6, Jul. 2005.

[5] L. Guo and Y. Chen, "Disk flutter and its impact on HDD servo performance," *IEEE Transactions on Magnetics*, vol. 37, no. 2, pp. 866-870, Mar. 2001.

[6] S. Imai, M. Tokuyama, and Y. Yamaguchi, "Reduction of disk flutter by decreasing disk-to-shroud spacing," *IEEE Transactions on Magnetics*, vol. 35, no. 5, pp. 2301-2303, Sept. 1999.

[7] B. Heo, I. Shen, and J. Riley, "Reducing disk flutter by improving aerodynamic design

of base castings," *IEEE Transactions on Magnetics*, vol. 36, no. 5, pp. 2222-2224, Sept. 2000.

[8] S. Deeyiengyang and K. Ono, "Suppressing of resonance amplitude of disk vibrations by squeeze air bearing plate," *IEEE Transactions on Magnetics*, vol. 37, no. 2, pp. 820-825, Mar. 2001.

[9] X. Huang, M. Hoque, X. Wang, and F. Yap, "A feedback control system for suppressing rotating disk flutter in hard disk drives," *Digest of the Asia-Pacific Magnetic Recording Conference 2002*, pp. AA5-01AA5-02, Piscataway, NJ, USA.

[10] G. Guo and J. Zhang, "Feedforward control for reducing disk-flutter-induced track misregistration," *IEEE Transactions on Magnetics*, vol. 39, no. 4, pp. 2103-2108, Jul. 2003.

[11] X. Wang and X. Huang, "Feedback control and optimization for rotating disk flutter suppression with actuator patches," *AIAA Journal*, vol. 44, no. 4, pp. 892-900, Apr. 2006.

[12] D. Oh and S. Kang, "Position error reduction in magnetic disk drives using a head gimbal assembly with radial head motion capability, " *Microsystem Technologies*, vol.11, no.8-10, pp. 728-33, Aug. 2005.

[13] M. Hayes, *Statistical Digital Signal Processing and Modeling*. New York: John Wiley & Sons Inc., 1996, ch. 9.

[14] M. Tomizuka, "Zero-phase error tracking algorithm for digital control," *ASME J. Dynamic Systems*, *Measurement and Control*, vol. 109, pp. 65-68, Mar. 1987.

[15] I. Landau, *System Identification and Control Design*. Prentice Hall, 1990, ch. V.

[16] L. Yi, "Two degree of freedom control for disk drive servo systems," Ph.D. dissertation, Dept. Mech. Eng., Univ. of California at Berkeley, Berkeley, CA, 2000.